JOURNAL OF THERMOPHYSICS AND HEAT TRANSFER
Vol. 8, No. 3, July–Sept. 1994

Hot-Gas-Side and Coolant-Side Heat Transfer in Liquid Rocket Engine Combustors

Ten-See Wang* and Van Luong†
NASA Marshall Space Flight Center, Huntsville, Alabama 35812

The objectives of this article are to develop a multidisciplinary, computational methodology to predict the hot-gas-side and coolant-side heat transfer in film cooling assisted, regeneratively cooled liquid rocket engine combustors, and to use it in parametric studies to recommend optimized design of the coolant channels for a developmental combustor. An integrated numerical model which incorporates computational fluid dynamics (CFD) for the hot-gas thermal environment, and thermal analysis for the liner and coolant channels, was developed. This integrated CFD/thermal model was validated by comparing predicted heat fluxes with those of hot-firing test and industrial design methods for a 40-k calorimeter thrust chamber and the Space Shuttle Main Engine main combustion chamber. Parametric studies were performed for the advanced main combustion chamber to find a strategy for a proposed coolant channel design.

Nomenclature

C_p = heat capacity
C_μ = turbulence modeling constant, 0.09
C_1 = turbulence modeling constant, 1.15
C_2 = turbulence modeling constant, 1.9
C_3 = turbulence modeling constant, 0.25
c = local speed of sound
D = dissipation terms
d = pipe diameter
E = empirical constant, 9.0
e = roughness height
F = convective flux
f = friction factor
G_{ij} = geometrical matrices, $(\partial\xi_i/\partial x_k)(\partial\xi_j/\partial x_k)/J$
H = enthalpy
h = heat transfer coefficient
J = Jacobian of coordinate transformation, $\partial(\xi_i, \xi_j)/\partial(x, y)$
J_n = diffusion fluxes for species n
K = thermal conductivity
k = turbulent kinetic energy
L = length
M = total number of chemical elements
MR = mixture ratio
m = mass flow rate
N = total number of species
Nu = Nusselt number
P_k = turbulent kinetic energy production
Pr = Prandtl number
p = static pressure
Q = heat flux
q = represents 1, u, v, h, k, and ε, and ρ_n
Re = Reynolds number
S_q = source term for equation q
T = static temperature
t = time
U_i = contravariant velocity, $(u_j/J)(\partial\xi_i/\partial x_j)$
u^* = friction velocity
u, v = mean velocities in x and y directions
W_n = mass production rate for species n
x, y = physical coordinates or distance
δ = grid cell or cross-sectional flow area
ε = turbulent kinetic energy dissipation rate
$\varepsilon_1, \varepsilon_2$ = dissipation parameters
κ = empirical constant, 0.4
λ = convective dissipation parameter
μ = effective viscosity
ν = artificial dissipation parameter
ξ = computational coordinates
ρ = density
σ_q = turbulence modeling constants
Φ = energy dissipation function
φ_c = curvature enhancement
φ_E = entrance enhancement
φ_R = roughness enhancement

Subscripts
b = bulk flow
c = coolant-side
fc = film coolant
g = hot-gas-side
l = laminar
t = turbulent
w = solid wall
wf = computational point next to the wall

Presented as Paper 92-3151 at the AIAA/SAE/ASME/ASEE 28th Joint Propulsion Conference, Nashville, TN, July 6–8, 1992; received Oct. 11, 1993; revision received Jan. 5, 1994; accepted for publication Jan. 6, 1994.

*Researcher, Computational Fluid Dynamics Branch. Member AIAA.
†Aerospace Engineer, Thermal Analysis Branch. Member AIAA.

Introduction

EVER since the development of rocket engines there has been a need to predict the peak heat flux from the combustion gases to the combustor wall to ensure the integrity of the combustion chambers. The continuous demand for higher performance engines has strengthened the need since higher pressures and temperatures are designed for the combustion chambers, and more sophisticated cooling methods such as regenerative cooling and film cooling have to be utilized. A coupled heat transfer problem among the hot-gas-side combustion chamber, the solid wall, and the coolant channels has therefore been created.

The long practice in the industry, however, has been using decoupled and simplified approaches. For example, a relaxation method is commonly used to analyze the solid wall

conduction heat transfer, whereas separate calculations are made for the combustion chambers and coolant channels using classical integral methods and empirical correlations. Those integral methods often assumed ideal flow conditions and subsequent corrections based on limited data base. The problem though, as pointed out by Bartz,[1] is that the real flow is characterized by numerous deviations from ideal flow described by a simplified model, and the differences are not small. Furthermore, the mixing characteristics of film coolant flow and bulk flow is probably too complex to be corrected with simple empirical correlations.

Computational fluid dynamics (CFD) has been developed to reduce the deviations of numerical models from real flow to a potential minimum. For example, multidimensional, multiple streams, turbulent, chemically reacting and recirculating flows can be considered. When CFD is used to model heat transfer, the need to assign velocity and temperature profiles is obviated because the actual fluid flow is calculated. The main objective of this study is therefore to propose a computational strategy that integrates both CFD and thermal analysis for the description of a coupled hot-gas/film, coolant/wall/coolant environment that occurs in most liquid rocket engine combustors. As a first attempt, the CFD model depicts the complicated hot-gas-side environment, whereas thermal models are used to analyze the solid wall heat conduction and the coolant-side flow environments. In general, the hot-gas-side wall serves as a common boundary between the hot gas and the solid liner and coolant channel flow, whereas the hot-gas-side wall temperature distribution was iterated until convergence. The heat fluxes for a 40-k calorimeter thrust chamber and the Space Shuttle Main Engine (SSME) were compared with those of several industrial methods and hot-fire tests. The effects of coolant channel aspect-ratio and wall thickness on wall surface temperature were studied for the advanced main combustor chamber (AMCC).

General Approach

The proposed computational methodology is composed of a CFD model for the hot-gas-side environment, a Systems Improved Numerical Differencing Analyzer (SINDA) thermal model for the solid wall heat conduction, and a SINDA-constructed, simplified flow model for the coolant channel flow environment. The CFD model solves an axisymmetric flowfield that predicts the near-wall thermal environments such as the local hot-gas temperature and heat flux to the chamber wall, including the mixing of bulk flow with the film coolant flow. The SINDA models describe a three-dimensional liner (liner, rib, and jacket) conduction heat transfer and a one-dimensional coolant channel flow; the liner wall temperature and thermal gradient, along with the coolant channel temperature and pressure drop, are determined. An initial hot-gas-side wall temperature distribution is usually assumed to start the CFD calculation, as shown in Fig. 1. For hydrogen-fueled rocket engine combustors, the radiative heat flux is negligible,[2] and the hot-gas-side heat flux is formulated as

$$Q_g = h_g(T - T_{gw}) \tag{1}$$

The coolant-side heat flux is given by

$$Q_c = h_c(T_{cw} - T) \tag{2}$$

For illustrative purposes, the temperature drops across the hot-gas, liner wall, and coolant can be written as

$$\begin{aligned}\Delta T &= \Delta T_g + \Delta T_w + \Delta T_c \\ &= Q_g/h_g + Q_w/(K/L) + Q_c/h_c\end{aligned} \tag{3}$$

After the CFD submodel is converged, the hot-gas-side heat flux is used as boundary condition for the thermal sub-models. A new hot-gas-side wall temperature distribution is returned from the thermal submodel calculations. The heat transfer from coolant-side jacket to the ambient air is negligible. The new hot-gas-wall temperature distribution is then served as the boundary condition for another hot-gas environment calculation. The modified near-wall environment is in turn used as a boundary condition for other thermal sub-model calculations. The hot-gas-side wall temperature distribution is iterated until $Q_g = Q_w = Q_c$. Approximately 5–10 global iterations are required to converge the whole integrated system.

A cutaway view of a typical, computational grid for the AMCC is shown in Fig. 2. The center piece is the CFD grid for the chamber, throat, and nozzle, whereas the outer shells are the SINDA grid for the liner and coolant channel. The coolant channel grid is clustered towards the hot-gas-side wall. For clarity, the combustor and liner grids are purposely separated. Those grids were constructed for illustrative purposes. In actuality, the CFD grid was an axisymmetric grid, whereas the three-dimensional SINDA grid (three-dimensionality is not shown) was only composed of half of a channel, due to symmetry. The model further assumes that the coolant was running at a constant transverse bulk temperature for a given axial location.

The hot-gas-side heat transfer coefficient is typically orders of magnitude larger than the thermal conductivity in the liner and the coolant-side heat transfer coefficient. This implies that the proposed integrated approach is more efficient than

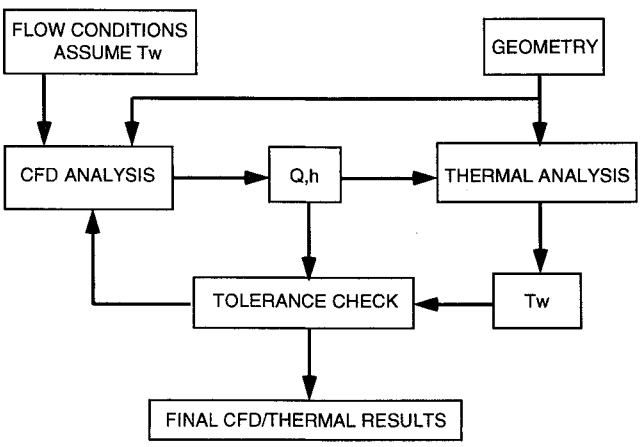

Fig. 1 Computational flow chart for the integrated CFD/thermal model.

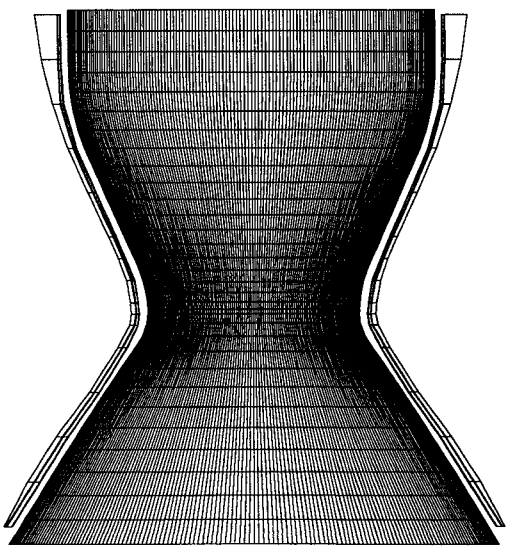

Fig. 2 Perpendicular cutaway view of the rotated CFD and SINDA computational grids for the AMCC calculation.

the conjugated approach since proven numerical techniques can be applied to both disciplines without encountering the computational stiffness problem. The modularity of the approach also allows readily testing and upgrading of the submodels. Furthermore, the same model and mesh used for thermal analysis can be used for a structural analysis.

Hot-Gas-Side Governing Equations

The basic equations employed in this study to describe the hot-gas environment with film cooling included in a liquid rocket engine combustor are the general-coordinate, multicomponent transport equations. A generalized form of these equations written in curvilinear coordinates is given by

$$\left(\frac{1}{J}\right)\left(\frac{\partial \rho q}{\partial t}\right) = \partial \frac{\left[-\rho U_i q + \mu G_{ij}\left(\frac{\partial q}{\partial \xi_j}\right)\right]}{\partial \xi_i} + \left(\frac{1}{J}\right) S_q \quad (4)$$

q represents 1, u, v, H, k, ε, and ρ_n, respectively. These are equations of continuity, x and y momentum, enthalpy, turbulent kinetic energy, turbulent kinetic energy dissipation rate, and density fractions. $\mu = (\mu_l + \mu_t)/\sigma_q$ is the effective viscosity when the turbulent eddy viscosity concept is employed to model the turbulent flows. $\mu_t = \rho C_\mu k^2/\varepsilon$ is the turbulence eddy viscosity, and C_μ and σ_q denote turbulence modeling constants. σ_q and S_q are given in Table 1.

In Table 1 C_1, C_2, and C_3 are model constants for the extended two-equation turbulence model.[3] The equation of state for an ideal gas is employed for the closure of the above system of equations. A four-step reversible hydrogen/oxygen equilibrium chemistry model[4] is used to close the combustion chemistry system. It consists of six species and four reactions as shown in Table 2.

Numerical Schemes

An adaptive upwind scheme was employed to approximate the convective terms of the momentum, energy, and continuity equations; the scheme is based on second- and fourth-order central differencing with artificial dissipation. First-order upwind scheme is used for the species and turbulence equations since the parameters involved must have positive quantities. Different eigenvalues are used for weighing the dissipation terms, depending on the conserved quantity being evaluated, in order to give correct diffusion fluxes near wall boundaries. Adding the dissipation term to F in ξ produces

$$\frac{\partial F}{\partial \xi} \simeq (F_{i+1} - F_{i-1})/2 - (D_{i+1/2} - D_{i-1/2}) \quad (5)$$

The dissipation terms are constructed such that a fourth-order central and fourth-order damping scheme is activated in smooth regions, and a second-order central and second-order damping scheme is used near shock waves. Since the Jacobian matrices of the Euler fluxes have eigenvalues of U, $U + c$ and $U - c$, it is sufficient to use the magnitudes of these eigenvalues to weigh the dissipation terms to maintain the smoothness of the solution without losing accuracy. $|U| + c$ was used for the continuity equation and $|U|$ was used for other transport equations in this study. General forms of the dissipation terms are given by—for the continuity equation

$$D_{i+1/2} = D_1(\rho_{i+1} - \rho_i) + D_2(\rho_{i-1} - 3\rho_i + 3\rho_{i+1} - \rho_{i+2}) \quad (6)$$

and for other transport equations

$$D_{i+1/2} = D_3(q_{i+1} - q_i) + D_4(q_{i-1} - 3q_i + 3q_{i+1} - q_{i+2}) + (1 - \varepsilon_1)(\rho U_{i+1/2}/16)[(q_i - q_{i-1}) - (q_{i+2} - q_{i+1})] \quad (7)$$

where

$$D_1 = 0.25\nu_{i+1/2}(|U| + c)_{i+1/2} \quad (8)$$

$$D_2 = \max(0, 0.01 - 0.25\nu_{i+1/2})(|U| + c)_{i+1/2} \quad (9)$$

$$D_3 = 0.5\varepsilon_1|\rho U|_{i+1/2} \quad (10)$$

$$D_4 = \varepsilon_2(1 - \varepsilon_1)\max[0.01\delta\rho(|u| + |v|), 2|\rho U|]_{i+1/2} \quad (11)$$

$$\varepsilon_1 = \max[\lambda, \min(1.0, 25\nu_{i+1/2})] \quad (12)$$

$$\varepsilon_2 = 0.015 \quad (13)$$

$$\nu_{i+1/2} = \max(a_i, a_{i+1}) \quad (14)$$

$$a_i = |p_{i+1} - 2p_i + p_{i-1}|/(p_{i+1} + 2p_i + p_{i-1}) \quad (15)$$

In the above formulations, unity λ corresponds to a full upwind differencing scheme for the momentum and energy equations, and vanishing λ corresponds to a central differencing scheme for the convective terms in smooth regions. δ stands for the local flow area.

A pressure-based predictor plus multicorrector solution method was employed so that a wide range of flow speeds could be analyzed with the same code. The basic algorithm of this pressure-based method is to perform corrections for the pressure and velocity fields by solving a pressure correction equation so that velocity and pressure coupling is enforced based on the continuity constraint at the end of each time integration step. The pressure correction equation is derived by combining a perturbed continuity equation, perturbed momentum equations, and a perturbed equation of state. The resulting pressure correction equation gives a mixed parabolic-hyperbolic form for subsonic flow and switches to a hyperbolic system for supersonic flow. This allows the flow solution to follow the flow characteristics and provides a smooth transition from low- to high-speed flow regimes. The time domain discretization of the present method allows the finite difference equation to be arranged into delta form for time marching integration. Details of the present numerical methodology are given in Refs. 4 and 5.

The chemistry source terms were evaluated with a point implicit procedure before the species equations were solved. The chemistry time step is synchronized with the flow time step and the temporal accuracy is preserved. In general, if there are N distinct chemical species composed of M chemical elements, the algebraic system to be solved consists of $N - M$ nonlinear equilibrium equations and M linear element-conservation relations. It has been shown[4] that a reduced system can be obtained by substituting the M linear relations into the $N - M$ nonlinear relations. As a result, an iterative

Table 1 σ_q and S_q of the transport equations

q	σ_q	S_q
1	1.00	0
u	1.00	$-p_x + \nabla[\mu(u_j)_x] - \frac{2}{3}(\mu\nabla u_j)_x$
v	1.00	$-p_y + \nabla[\mu(u_j)_x] - \frac{2}{3}(\mu\nabla u_j)_y$
H	0.95	$Dp/Dt + \Phi + \Sigma J_n C_{pn}\nabla T - \Sigma H_n W_n$
k	0.89	$\rho(P_k - \varepsilon)$
ε	1.15	$\rho(\varepsilon/k)(C_1 P_k - C_2\varepsilon + C_3 P_k^2/\varepsilon)$
ρ_n	1.00	$W_n,\ n = 1, \ldots, N$

Table 2 Reactions

Reactions
$O_2 = 2O$
$H_2 = 2H$
$2OH = O_2 + H_2$
$2H_2O = 2H_2 + O_2$

Newton-Raphson technique was used to solve a system of $N - 2M$ equations rather than the larger equivalent $N \times N$ system. Utilizing this system reduction method, the six unknowns, two element-conservation equations plus four nonlinear equilibrium chemistry equations system can be reduced. The final reduced system consists of one cubic equation and one quadratic equation with two unknowns, and can readily be solved by Newton-Raphson's iterative method.

Boundary Conditions

Fixed chamber total conditions were used at the inlet of the combustion chamber. The static pressure wave is allowed to propagate upstream of the inlet by extrapolation. This is to allow the transient disturbances sent from downstream to permeate through the boundary. The propellant flow is assumed to be fully turbulent at the injector faceplate in order to take advantage of the high Reynolds number k-ε turbulence equations.[6] Flow properties at the wall, centerline, and exit were extrapolated from those of the interior domain. Near the combustor wall surface, the standard wall function approach[6] was used to provide boundary conditions for the momentum and energy equations and the turbulence model. That is, for the k equation the turbulent kinetic energy dissipation rate is modeled as

$$\varepsilon_{wf} = C_\mu^{3/4} k_{wf}^{3/2} / (y_{wf}\kappa) \; // \; (E\rho y_{wf} u^*/\mu) \tag{16}$$

The turbulent boundary layer started from the injector faceplate may laminarize due to the effect of flow acceleration on turbulence. If laminarization occurs there will be a reduction in heat transfer, and a low Reynolds number turbulence model should be used or appropriate wall functions should be developed. A previous study[7] has found that when the acceleration parameter K factor (evaluated at the edge of the boundary layer) exceeded about 2×10^{-6}, where

$$K \text{ factor} = \left(\frac{\mu}{\rho u^2}\right)\left(\frac{du}{dx}\right) \tag{17}$$

heat transfer was reduced below values typical of turbulent boundary layers. This criterion is used in this work to determine if laminarization can occur in a given combustion chamber.

Figure 3 shows that the calculated acceleration parameters for all three combustors used in this study are less than 2.0×10^{-6} along the combustor walls. The assumption of turbulent flow throughout the combustors is therefore considered to be appropriate for the purpose of this work.

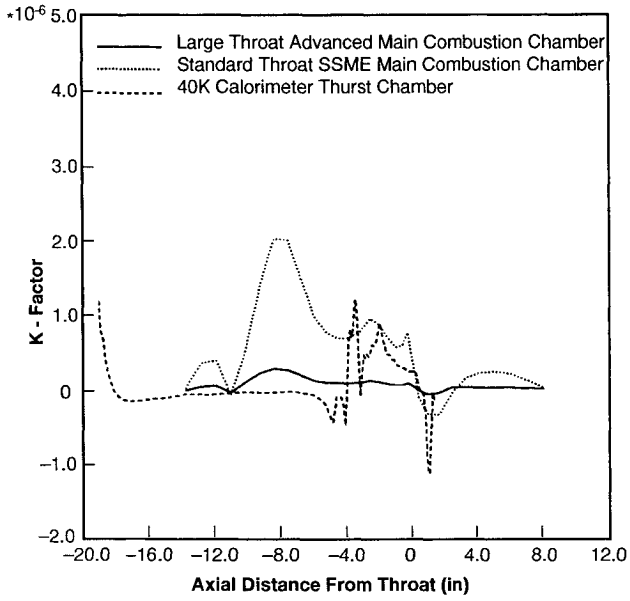

Fig. 3 Acceleration parameters for the three combustors of interest.

Thermal Model Description

A three-dimensional heat conduction model for the liner and a one-dimensional hydraulic model for the coolant channel have been constructed using SINDA. The SINDA code has been used for many years in these applications such that the analytical methods have been well verified. It is a software system with capabilities that makes it well-suited for solving lumped parameter representations of physical problems governed by diffusion-type equations. The system is designed as a general thermal analyzer accepting resistance-capacitance (R-C) network representations of thermal systems.

Inputs to the thermal model include dimensions of the combustion chamber and coolant channel, local hot-gas temperature and heat transfer coefficient, coolant inlet temperature and heat transfer coefficient, upstream and downstream manifold pressures, and types of materials used for the chamber liner and jacket. The outputs include the wall temperatures, temperature gradients across the liner walls, mass flow rates, coolant temperature, and pressure distribution throughout the coolant channel. Parametric studies on combustion chamber contours, coolant channel dimensions, number of coolant channels, and wall thickness have been performed.

Liner Model

The liner wall was modeled using SINDA as discussed in Ref. 8. The liner model of combustion chamber is divided into many axial stations from inlet manifold to outlet manifold. Each station has typically 51 mass nodes in circumferential and radial directions. Axial, circumferential, and radial wall temperature distributions were obtained from this model.

Coolant Channel Model

The SINDA code has also been used to construct a one-dimensional hydraulic model for coolant channel flow. An R-C network method in SINDA was again used for modeling this fluid flow which can be coupled readily to the liner model. The governing equations for general incompressible and compressible pipe flows were developed for SINDA[9] and have been used for this analysis. The incompressible flow equations were used for the 40-k calorimeter thrust chamber calculation since the working fluid is water, while the compressible flow equations were used for the standard throat (ST) SSME main combustor chamber (MCC) and large throat (LT) vacuum plasma spray (VPS) AMCC calculations since the working fluids are hydrogen.

Once the coolant flow rate, velocity, temperature, and pressure are determined, the coolant heat transfer coefficient can be evaluated. The Dipprey and Sabersky's[10] correlation was used for hydrogen coolant:

$$Nu = \frac{(f/8)RePr(T_b/T_w)^{0.55}\varphi_c\varphi_E}{\{1 + (f/8)^{0.5}[B(\varepsilon^*) - 8.48]\}} \tag{18}$$

$$\varepsilon^* = Re(e/d)(f/8)^{0.5} \tag{19}$$

$$B(\varepsilon^*) = 4.7(\varepsilon^*)^{0.2} \quad \text{for} \quad \varepsilon^* \geq 7 \tag{20}$$

$$B(\varepsilon^*) = 4.5 + 0.57(\varepsilon^*)^{0.75} \quad \text{for} \quad \varepsilon^* < 7 \tag{21}$$

where e/d is the relative roughness. Fluid properties for the above correlation were based on the bulk temperature and pressure.

When the coolant is water, the Dittus-Boelter's correlation[11] for smooth surface and fully developed turbulent pipe flow is used:

$$Nu = 0.023Re^{0.8}Pr^{0.4}\varphi_c\varphi_R\varphi_E \tag{22}$$

Fluid properties for the above correlation were based on the film temperature and pressure. The enhancement factors for the above correlations were obtained from Ref. 12.

Results and Discussion

40-k Calorimeter Thrust Chamber Calculation

At NASA Marshall Space Flight Center (MSFC), a calorimeter chamber of modular design was used for evaluating and comparing injector and chamber designs. This pressure-fed system was rated at 40,000 lb of thrust for a chamber pressure of 3000 psia. Selected hot-firing test data has been used for our model validation. In particular, steady-state analysis was performed with test configuration no. 3.[13] The computational model includes the 3.5-in. transition, 8-in. spool, 2-in. adaptor spool, and 6.6-in. throat sections. All chamber components were circumferentially cooled by water. They were manufactured with a Wrought Narloy-Z (a copper alloy) material except for the 8-in. spool, which had a Narloy-Z liner made with a VPS process, a nickel closeout over the coolant channels, and a stainless steel housing. These materials were all considered in the thermal model. The hot-gas-side calculating parameters for the 40-k test, along with those of the ST SSME MCC and LT VPS AMCC, are shown in Table 3. Approximately 5% of the fuel flew at the chamber wall as added film cooling. The coolant inlet pressure was 4600 psia, and the coolant inlet temperature was about 60°F. The coolant flow rate was varied for each coolant circuit.

Figures 4 and 5 show the comparisons of the predicted coolant discharge temperature and the heat flux with those of the measurements[13] from the 40-k calorimeter thrust chamber hot-fire test. The comparisons agreed reasonably well, especially at or near the throat region, where the maximum coolant discharge temperature and the peak heat flux occurred. However, the model somewhat overpredicted the coolant discharge temperature and the heat flux at the barrel section of the combustor. It was speculated that the reported misalignment[13] of the outer row liquid oxidizer injection post of the test article may have contributed to that discrepancy. The initial heat flux near the injector faceplate was sensitive to the film coolant flow properties. This implies that film cooling is responsible for the low heat flux near the injector faceplate.

Table 3 Hot-Gas-Side calculating parameters

	p, psia	m_b, lbm/s	m_{fc}, lbm/s	MR
40-k test	1568	64.3	3.8	6.87
ST SSME MCC	3276	1129.6	4.84	6.01
LT VPS AMCC	3021	1140.0	1.07	6.01

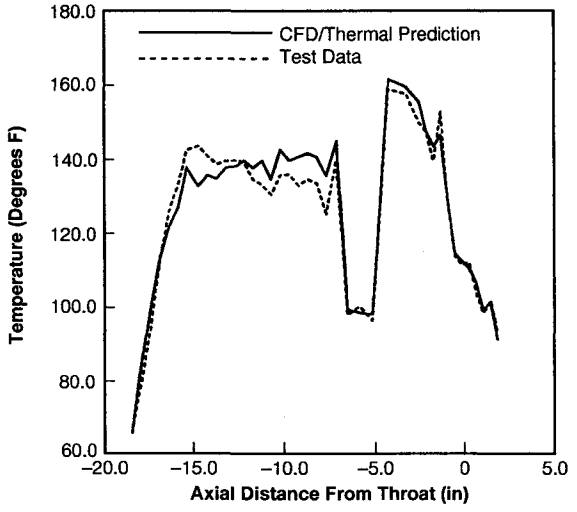

Fig. 4 Coolant discharge temperatures for the 40-k calorimeter thrust chamber.

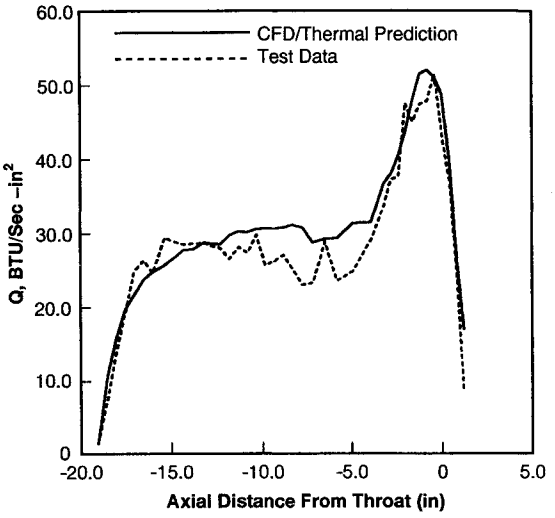

Fig. 5 Hot-gas-side wall heat fluxes for the 40-k calorimeter thrust chamber.

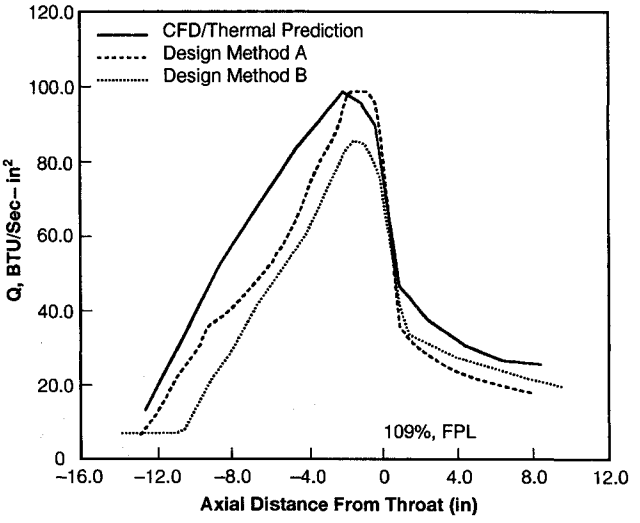

Fig. 6 Comparison of the predicted heat flux distributions for the ST SSME MCC.

Standard Throat SSME MCC Calculation

The calculation was performed at SSME full power level (FPL) operating condition (109%). The current SSME MCC consists of a coolant liner which is made of Wrought Narloy-Z. The liner provides the coolant flow path for the MCC. It has 390 milled axial coolant channels that are closed out by an electroforming process which deposits a copper barrier, followed by a nickel closeout over the coolant channels. The coolant flow rate was 31.54 lb/s, which was determined from a engine power balance calculation.[14]

Figure 6 shows the comparison of the predicted wall heat flux at FPL with those of other design[15,16] methods. Design method A used a one-dimensional calculation for the hot-gas-side flow and corrected the upstream adiabatic wall temperature[17] by adjusting for the influence of film coolant flow. For the coolant-side flow, a REGENerative-cooling design/analysis code[18] was used to balance the heat. Marshall Space Flight Center's 40-k calorimeter test data was scaled to full power level as the empirical data base. Design method B used similar methodology to predict the wall heat flux.

Since the measured axial heat flux for the SSME MCC is not available, the comparison of the trends is more meaningful than the absolute magnitudes. In general, the trend was similar for these methods. Specifically, the predicted peak heat fluxes are quite close for the CFD/thermal model and design method A. Design method B predicted lower peak heat flux, possibly due to its usage of a higher film coolant flow rate.

All three predicted peak heat fluxes occurred just before the throat region, where it is most susceptible to chamber blanching or cracks. Overall, mismatches occurred between the throat and the injector face plate. This is probably due to the difference in estimating the film coolant boundary-layer effect. Figure 7 shows the CFD/thermal model predicted hot-gas-side wall temperature profile. The maximum surface temperature (1080°F) is below the critical temperature (1100°F).

Figure 8 shows the predicted coolant temperature and pressure profiles. The coolant is heated from 97°R at the coolant channel inlet, to about 460°R at the exit. The corresponding coolant channel pressure enters at 6461 psi, and drops to 5137 psi at the outlet of the channel.

Large Throat VPS AMCC Calculation

The proposed LT VPS AMCC[19] is modified from the SSME MCC. By enlarging the throat area, the nozzle expansion ratio is reduced from 77.5 to 69.5. The chamber pressure at FPL is reduced from 3276 to 3021 psia, as shown in Table 3. The film coolant flow rate was also reduced. It has a Narloy-Z liner made with the VPS process, a JBK-75 closeout over the coolant channels. In addition, there is some difference in throat radius of curvature, for both the upstream and downstream locations, between the two designs.

Design sensitivity studies have been performed for AMCC on the effects of the number of coolant channels and the wall thickness. Figure 9 shows the comparison of the AMCC hot-gas-side wall temperatures for 430 channels (present design) and 550 channels (redesign). The maximum aspect-ratio for the 550-channel case is 7.8, and it is 5.0 for the 430-channel case. The minimum channel width has been decreased from 0.035 to 0.021 in., while the minimum wall thickness and the coolant pressure drop remain the same. The coolant mass flow rate is 29.45 lb/s, and the pressure drop is 1307 psi.[20] It can be seen that increased aspect ratio and more coolant channels reduce the hot gas surface wall temperature and thermal gradient. This is caused by a significant increase in surface contact area and heat transfer between the coolant and liner wall. The coolant inlet temperature is 97°R. The coolant outlet temperature is 490°R for the present design and 520°R for the redesign. The reduced hot gas surface wall temperature and thermal gradient imply less chance for wall blanching and cracks for the 550-channel design. The effect of wall thickness on heat transfer is shown in Fig. 10. Clearly, a reduction in wall thickness improves the cooling efficiency, and vice versa. However, wall thickness that is reduced to less than the critical limit could result in the reduction of MCC life.

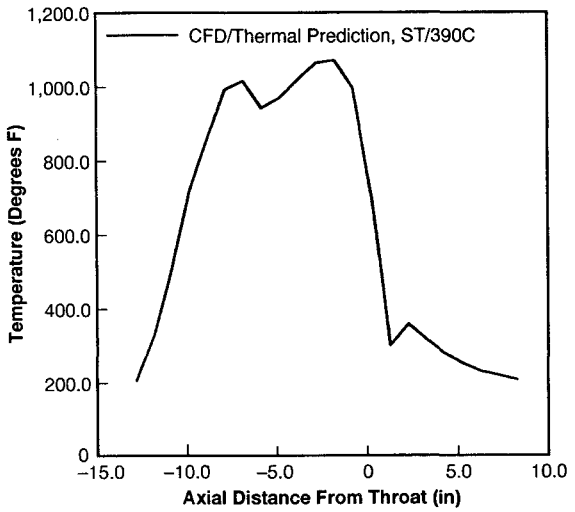

Fig. 7 Predicted hot-gas-side surface temperature for the ST SSME MCC.

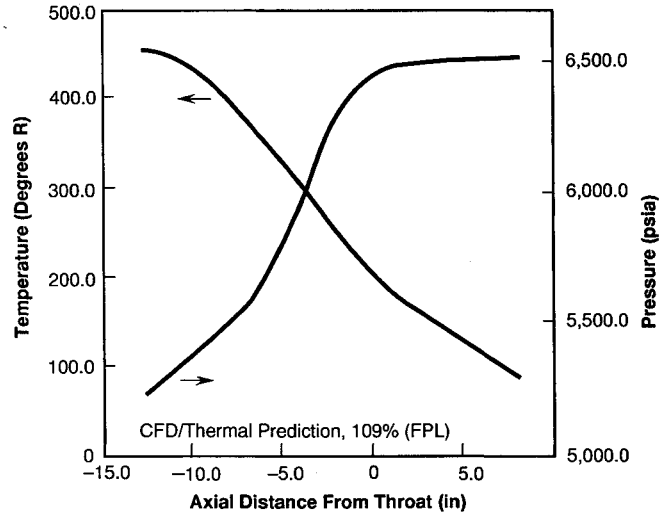

Fig. 8 Predicted coolant channel temperature and pressure distributions for the ST SSME MCC.

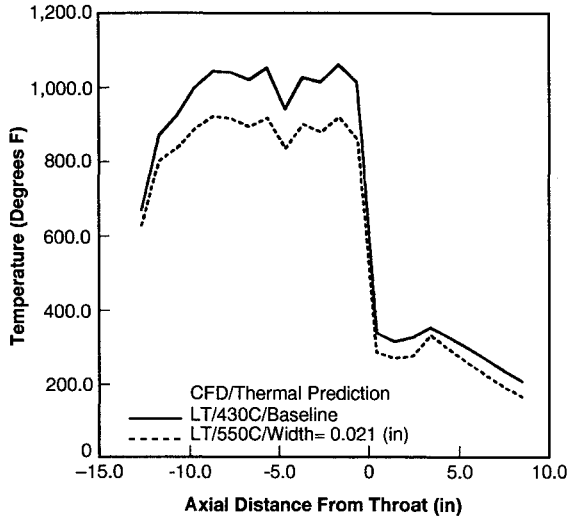

Fig. 9 Comparison of the AMCC hot-gas-side surface wall temperatures for 430 and 550 channels.

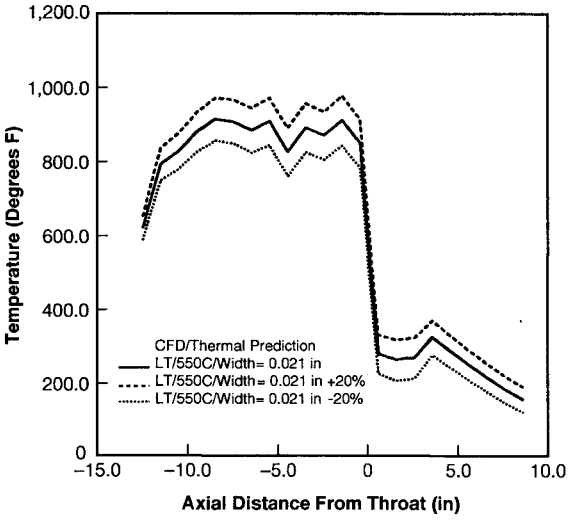

Fig. 10 Comparison of the AMCC hot-gas-side wall temperatures for wall thickness sensitivity study.

Conclusions

An integrated CFD/thermal methodology has been developed to design and analyze regeneratively cooled rocket engine combustion chambers. The procedure involved iterating

around a common boundary (hot-gas-side temperature distribution) between a CFD submodel and two thermal submodels. The CFD model describes the hot gas environment and the thermal models depict the liner and the coolant channel environments. The predicted wall heat flux compared well with that measured from a 40-k calorimeter thrust chamber tester.[13] Film cooling was responsible for the low heat flux near the injector faceplate. When applied to the SSME MCC, the model-predicted heat flux compared reasonably well with those of other industrial design methods.[15,16] Parametric studies were also performed for a proposed AMCC coolant channel design. It is found that increased aspect ratio and number of coolant channels reduce the peak wall temperature and thermal gradient. Furthermore, a 20% reduction of the wall thickness also improved the cooling efficiency. However, a reduction of the wall thickness may reduce the liner life.

References

[1]Bartz, D. R., "Turbulent Boundary-Layer Heat Transfer from Rapidly Accelerating Flow of Rocket Combustion Gases and Heated Air," *Advances in Heat Transfer*, edited by J. P. Hartnett and T. F. Irvine Jr., Academic Press, New York, Vol. 2, 1965, pp. 1–108.

[2]Chou, L.-C., Mo, J.-D., Liaw, G.-S., and Wang, T.-S., "A Radiation Modeling for the SSME Combustor/Nozzle Flowfield," 9th CFD Workshop Meeting, NASA/MSFC, Huntsville, AL, April 1991.

[3]Chen, Y.-S., and Kim, S.-W., "Computation of Turbulent Flows Using an Extended k-ε Turbulence Closure Model," NASA CR-179204, Oct. 1987.

[4]Wang, T.-S., and Chen, Y.-S., "Unified Navier-Stokes Flowfield and Performance Analysis of Liquid Rocket Engines," *Journal of Propulsion and Power*, Vol. 9, No. 5, 1993, pp. 678–685.

[5]Wang, T.-S., "Numerical Study of the Transient Nozzle Flow Separation of Liquid Rocket Engines," *Computational Fluid Dynamics Journal*, Vol. 1, No. 3, 1992, pp. 319–328.

[6]Patankar, S. V., and Spalding, D. B., *Heat and Mass Transfer in Boundary Layers*, 2nd ed., Intertext Books, London, 1970.

[7]Back, L. H., Cuffel, R. F., and Massier, P. F., "Laminarization of a Turbulent Boundary Layer in Nozzle Flow-Boundary Layer and Heat Transfer Measurements with Wall Cooling," *Journal of Heat Transfer, Transactions of the American Society of Mechanical Engineers*, Series C, Vol. 92, Aug. 1970, pp. 333–344.

[8]Gaski, J., "The Systems Improved Numerical Differencing Analyzer (SINDA) Code—a User's Manual," Aerospace Corp., El Segundo, CA, Feb. 1986.

[9]Owen, J. W., "N-Dimensional Fluid Networks Approach Within SINDA," *Thermal Analysis Workbook*, NASA, Marshall Space Flight Center, Huntsville, AL, 1991.

[10]McCarthy, J. R., and Wolf, H., "The Heat Transfer Characteristics of Gaseous Hydrogen and Helium," Rocketdyne Div. of North American Aviation, Research Rept. RR-60-12, Canoga Park, CA, 1960.

[11]Incropera, F. P., and DeWitt, D. P., *Fundamentals of Heat and Mass Transfer*, 2nd ed., Wiley, New York, 1985.

[12]Niino, M., Kumakawa, A., Yatsuyanag, N., and Suzuki, A., "Heat Transfer Characteristics of Liquid Hydrogen as a Coolant for the LO_2/LH_2 Rocket Thrust Chamber with the Channel Wall Construction," AIAA Paper 82-1107, June 1982.

[13]Elam, S. K., "Subscale LOX/Hydrogen Testing with a Modular Chamber and a Swirl Coaxial Injector," AIAA Paper 91-1874, June 1991.

[14]Neumeyer, R. K., "Release of Updated SSME Phase II Nominal Engine Power Balance and Operating Maximums Handbook," Rockwell International, IL 90-05-012, Canoga Park, CA, Jan. 31, 1990.

[15]Romine, W. D., personal communication, Rocketdyne, Canoga Park, CA, 1990.

[16]Peckham, R., personal communication, Pratt and Whittney, West Palm Beach, FL, 1990.

[17]Hatch, J., and Papell, S. S., "Use of a Theoretical Flow Model to Correlate Data for Film Cooling or Heating an Adiabatic Wall by Tangential Injection of Gases of Different Fluid Properties," NASA TND-130, Nov. 1959.

[18]Gerstley, J. G., Wagner, W. R., Pidcoke, L. H., and Tobin, R. D., "REGENerative Cooling Design/Analysis Computer Program," Rocketdyne, Rockwell International, ASR 73-170, Canoga Park, CA, 1973.

[19]Tygielski, K., "Advanced Technology Application for Combustion Chamber Concepts," AIAA Paper 92-3857, July 1992.

[20]Neumeyer, R. K., and Davidson, D. M., "Large Throat Interim Nominal Engine Power Balance," Rockwell International, IL 90-05-044, Canoga Park, CA, Oct. 1990.